General Method to Construct Flat Bands in Two-Dimensional Lattices

H. T. Li, T. Z. Ji, R. G. Yan, W. L. Fan, Z. X. Zhang, L. Sun,
B. F. Miao, G. Chen, X. G. Wan, and H. F. Ding[*]
*National Laboratory of Solid State Microstructures, Department of Physics, and
Collaborative Innovation Center of Advanced Microstructures, Nanjing University, Nanjing 210093, China*

Searching for new materials hosting flat bands is pivotal for exploring strongly correlated effects and designing sensitive quantum devices, but remains challenging. We present a general method for realizing flat bands based on mathematical optimization and symmetry analysis. The method enables the discovery of ~1000 types of two-dimensional lattices that can host flat bands, in sharp contrast with ~10 flat-band lattices predicted previously besides the well-known ones. We further verify the method using first-principles calculations. Our approach provides new insights for the design of flat-band lattices, particularly when aiming to create experimentally feasible configurations.

Flat bands have emerged as a central topic in condensed matter physics and materials sciences [1–5]. Owing to their unique dispersionless energy-momentum relation, electrons in flat bands possess vanishing group velocity and a divergent effective mass, resulting in negligible kinetic energy [6,7]. Consequently, weak interactions or disorder cannot be treated as perturbations. Thus, flat-band systems can be exceptional platforms for investigating strongly correlated effects and designing extraordinarily sensitive quantum devices. Since the discovery of ferromagnetism induced by the Hubbard interaction [8,9], extensive studies have been carried out to investigate the exotic physics of flat bands, such as Anderson localization [10], disorder-induced multifractality [11], topological phase transitions [12], mobility edges [13], compact breathers under nonlinearity [14], and superconductivity [15], etc.

Given the significance of flat-band systems, various methods have been proposed for constructing systems containing flat bands. Essentially, they can be classified into two categories. Brute-force search approaches screen for flat-band materials from the first-principles material databases [16–18] or the k-uniform tiling database [19,20]. These methods have yielded fruitful outcomes, extensively categorizing most known materials and establishing comprehensive databases. However, they lack the capability to design new materials and to control the energy of flat bands. An additional strategy is needed to tune the flat bands to the desired energy. Other methods, such as origami rules [21], local unitary transformations [22,23], line graphs [9,24–27], miniarrays [28], chiral symmetry [29], local symmetry [30], latent symmetry [31], embedding mechanism [32], etc., involve constructing specialized Hamiltonian matrices and

mapping them onto lattices to achieve flat bands. These methods rely on solving a series of constraint equations to meet the requirement of destructive interference of the electron wave functions. These efforts have successfully constructed certain flat-band lattices. The results, however, are still rather limited. Only ~10 new flat-band lattices, besides the well-known ones, were obtained. Some of them were obtained by assuming that the next nearest-neighbor (NN) hopping is either negligibly small or even larger than the NN hopping, which is challenging to realize in real systems.

Recently, two-dimensional (2D) materials have attracted widespread attention due to their unique properties and the rapid expansion of the materials repertoire. Owing to the van der Waals bonding between layers, they can be assembled in a LEGO-like manner to produce rich novel materials, including flat-band structures [33–41]. Furthermore, through atomic manipulation or molecular self-assembly, researchers can construct materials that do not naturally exist at the atomic scale and investigate their exotic properties [1,42–50]. Similarly, other approaches can be used to construct new materials in a designed manner, such as the optical waveguide networks [51–53], exciton-polariton condensates [54,55], and ultracold atomic condensates [56–58]. These engineered materials are stabilized by the supporting substrate or optical potential well, etc. With high tunability, they significantly broaden the parameter space for searching flat-band lattices. Apparently, not all lattices possess flat bands, and these kinds of experiments are typically expensive and time-consuming. This underscores the need for an efficient method to design flat-band lattices before carrying out real experiments.

Here, we demonstrate a general flat-band generator using a nonlinear programming method. Essentially, we utilize two strategies to simplify the complexity of the problem.

*Contact author: hfding@nju.edu.cn

First, we reduce the uncertainty associated with hopping by using preestablished distance-dependent overlap energy. Second, we impose symmetry constraints during the flat-band lattice generation process, further narrowing the search space for the site positions. As a result, the task of constructing the flat-band lattice can be completed in a short time. Utilizing two typical dependencies, we search for lattices exhibiting flat bands across all 2D space groups. Remarkably, in both cases, we find ~1000 flat-band lattices [structures and band details are provided in the Supplemental Material (SM) [59]] for the number of sites within a unit cell no more than 11, indicating that they are more abundant than commonly thought. We further verify our approach using first-principles calculations. Our method paves a new avenue for the design of flat-band lattices, particularly when creating experimentally feasible configurations.

We first utilize two typical examples to illustrate our approach. The first one is the kagome lattice, whose unit cell contains three sites [Fig. 1(a)]. For a lattice containing n sites in a unit cell with the primitive translational vectors R_1, R_2, the position of site i in cell l (2D index) can be written as $\mathbf{r}_{l,i}$. The Hamiltonian of the system can be written as

$$H = \sum_{l,i} \mu_i c_i^\dagger c_i - \sum_{l,i} \sum_\delta J_\delta (c_{l,i}^\dagger c_{(l,i)+\delta} + \text{H.c.}), \quad (1)$$

where μ_i denotes the on-site energy at site i, and J_δ is the overlap integral between neighboring sites. $c_{l,i}^\dagger$ and $c_{l,i}$ stand for the fermionic creation and annihilation operators at $\mathbf{r}_{l,i}$, respectively. For a kagome lattice with the NN hopping, J_1 only, its band structure shows a flat band at $E = -2J_1$ when $\mu_i = 0$ [Fig. 1(b)]. This is the well-known electronic structure of a kagome lattice and can be readily generated using our newly developed flat-band lattice generator, as illustrated below. Similarly, complex lattices generated by our flat-band lattice generator can also possess flat bands. For example, in Fig. 1(c), where the hopping between atoms follows a distance dependence as $J_\delta \propto (1 + d/a_0)e^{-d/a_0}$ (similar to the hopping between the $1s$ states of two hydrogen atoms [63]), where a_0 is the Bohr radius, and d is the distance between two hopping sites, namely $d = |\mathbf{r}_{l,i} - \mathbf{r}_{(l,i)+\delta}|$. The corresponding energy bands [Fig. 1(d)] reveal two flat bands, highlighted in orange.

Based on the above two examples, we find that the energy bands are entirely determined by R_1, R_2, the positions of each site within a unit cell, $\mathbf{r}_{l,i} - R_l$ and J_δ, which depends on the relative positions between the hopping sites. With a known distance-dependent hopping $J(d)$, the energy bands are completely determined by positions of the sites. Through a Fourier transform, the Hamiltonian in Eq. (1) can be converted to a Hamiltonian in k-space: $H(\mathbf{k})$ (SM Note 1). Solving the eigenvalue problem yields the energy bands
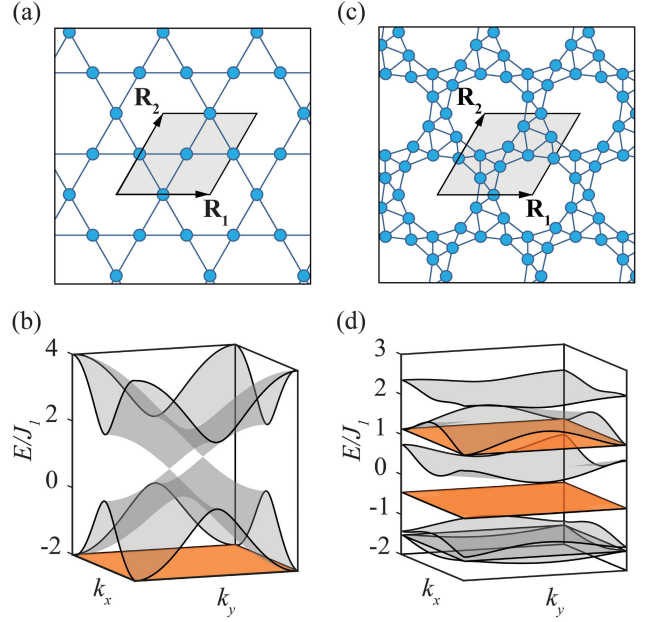

FIG. 1. Two examples of the flat-band lattices and their corresponding band structures. (a) Structure of a kagome lattice. (b) Energy band of a kagome lattice with the NN interaction J_1 only, showing a flat band at $E = -2J_1$. (c) Structure of a complex flat-band lattice designed by our flat-band generator with its energy band containing two flat bands as shown in (d). Flat bands are highlighted in orange.

$$\det |H(\mathbf{k}) - \varepsilon I| = 0 \quad (2)$$

To obtain flat-band lattices, it is natural to choose the energy bandwidth ΔE of each band as the evaluation function. The objective is to minimize ΔE below a given threshold by adjusting R_1, R_2, and $\mathbf{r}_{l,i} - R_l$. To find as many flat-band lattices as possible, we repeat the process for every band and also crosscheck the lattice to avoid double-counting when more than one flat band was found in a lattice. In this work, we utilize the simulated annealing (SA) method [64–66], an algorithm commonly used for finding optimal solutions to various optimization problems. Therefore, we refer to our method as the SA flat-band (SA-FB) generator.

As shown in the diagram in SM Note 2, our SA-FB generator begins with a random lattice. In each iteration, it calculates ΔE of the new lattice generated through the random walk and updates a temporary ΔE_{temp} according to the Metropolis sampling rule with a certain probability. In the end, the results are classified based on ΔE_{min} (the minimum of ΔE_{temp}) of the best solution.

Figure 2(a) presents the ΔE-*step* curve, with the corresponding evolution of the positions of the lattice sites shown in Fig. 2(b). It shows that ΔE_{min} and the fluctuation of ΔE_{temp} decreases to almost zero. By comparing the initial lattice and its corresponding band structure [Figs. 2(c) and 2(d)] with the typical intermediate configuration
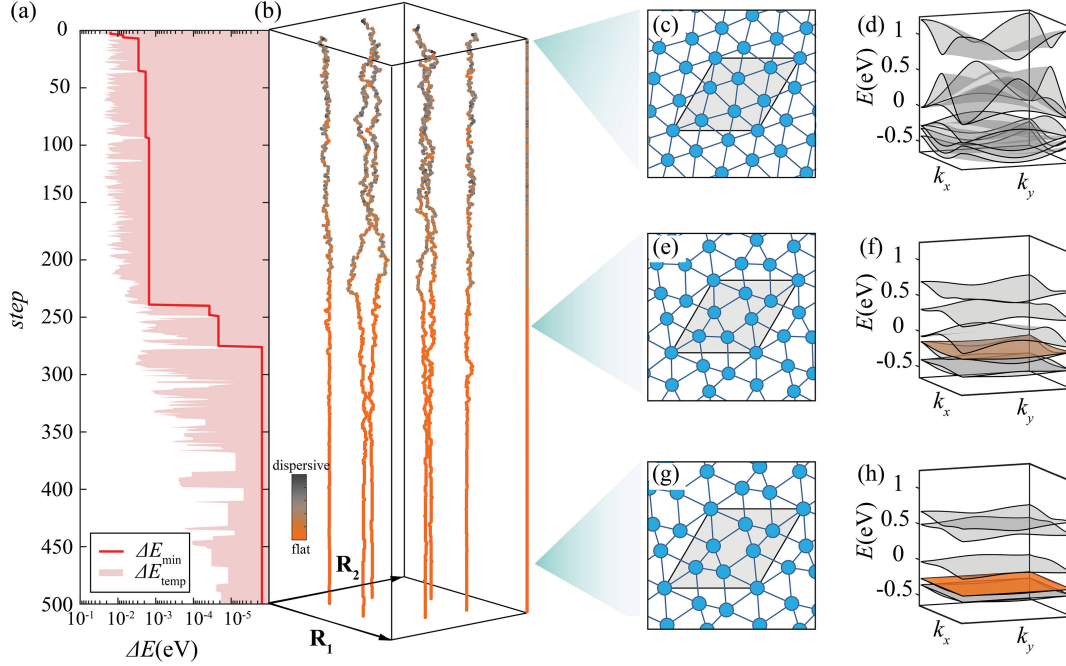
FIG. 2. Process of generating a flat band using the SA-FB generator. (a) Evolution of ΔE_{temp} and ΔE_{min} with the iterations. (b) Random walk trajectories of the individual sites. (c) Initial configuration of the lattice, (d) the corresponding band structure of panel (c), which contains no flat band. (e), (f) Intermediate lattice configuration, and its corresponding band structure, which contains a narrow dispersive band. (g), (h) Final lattice configuration and its corresponding band structure, which contains a flat band highlighted in orange.

[Figs. 2(e) and 2(f)] and the final lattice [Figs. 2(g) and 2(h)], it is evident that the SA-FB generator does gradually achieve a flat band (marked in orange) by fine-tuning the positions of the sites.

Existing works have shown that flat bands are closely related to symmetry [16,27,30], our SA-FB generator constrains the lattice under a specific 2D space group to improve efficiency. In each iteration, one of the sites attempts a random walk while preserving symmetry. To achieve this, we classify the site positions into three different types and impose specific rules for each type individually (SM Note 2).

In the calculation, it is important to consider higher-order NN hopping terms. The calculation, however, becomes impractical if all possible hopping between any two sites is included. To maintain computational efficiency while capturing the essential physics, two additional rules are applied: (1) the threshold rule, which states that since weak hopping has negligible impact on the band structure, all hopping below a certain threshold (e.g., $J(d) < (J_1/10)$) is discarded. Note that the threshold can be adjusted depending on specific requirements. (2) The modulating rule, which states that if the hopping path is too close to any site, the hopping is subject to being scattered and is considered as modulated. In such a case, the hopping strength is multiplied by a factor of α from the original value without being scattered. For simplicity, we mainly discussed the results for $\alpha = 0$ but the main conclusion does not change for $\alpha \in [0, 2]$ (see SM Note 3).

We apply our SA-FB generator to all different 2D space groups. In these processes, we utilize the distance-dependent hopping between two hydrogen atoms, specifically $J(d) \propto (1 + d/a_0)e^{-d/a_0}$, and set the NN distance to be $6.5a_0$, which can be modified as needed. When ΔE_{min} is between 10^{-11} and 1 meV or below 10^{-11} meV, the lattices are classified as the quasi-flat-band or strict-flat-band lattices, respectively. The 1 meV threshold is chosen because it is difficult to resolve it with most current experimental techniques, while 10^{-11} meV is below the floating point error. We summarize the results for each group in Table I and list their details in the SM. Remarkably, we find 1021 lattices containing flat bands, far exceeding common expectations. Even when limiting the discussion to the strict-flat-band lattices, there are still over 700. We also made the inverse participation ratio calculations for all the obtained flat bands (SM Note 4) and confirmed they are all true flat bands that delocalized over many sites. The flat bands in these lattices are almost continuously distributed from ~ -0.5 eV to 0.4 eV, making it possible to customize the energy where the flat band appears within a certain range by choosing the corresponding flat-band lattice (see SM Note 5). Notably, with respect to this specific distance dependence, half of them belong to the $p3$ group, while none belong to the $p1$ and $c2mm$ groups. These results highlight the significant role of symmetry constraints. In $p1$ lattices, which lack any form of rotational symmetry, finding suitable optimization directions toward fully destructive interference could be challenging for this

TABLE I.   List of $(1 + d/a_0)e^{-d/a_0}$-dependence design results.

Group	Quasi	Strict	Total
$c1m1$	28	1	29
$p1$, $c2mm$	0	0	0
$p1g1$	39	44	83
$p1m1$	36	25	61
$p2$	84	23	107
$p2gg$	66	72	138
$p2mg$	16	40	56
$p2mm$	8	63	71
$p3$	24	330	354
$p31m$	0	12	12
$p3m1$	0	36	36
$p4$	6	19	25
$p4gm$	1	0	1
$p4mm$	0	25	25
$p6$	0	3	3
$p6mm$	0	20	20
Total	308	713	1021

hopping dependence. As a result, flat-band structures are not found. Conversely, when symmetry constraints are extreme, as observed in lattices belonging to the $c2mm$, $p4gm$, $p6$, and $p6mm$ groups, the sites can only be adjusted within very limited ranges, resulting in similar lattice configurations. If these lattices do not inherently possess flat bands, achieving a flat-band lattice becomes nearly impossible. Thus, only a limited number of flat-band lattices are found. Interestingly, apart from the lattices containing one or two flat bands, we also find some all-band-flat lattices in which all bands are dispersionless [11] (see SM Note 6).

To demonstrate the generality of our approach, we also apply the SA-FB generator to a $(1/d^2)$-dependence model, which was recently discovered in the system of $3d$ transition metal adatoms on a noble metal surface with surface states, such as Fe adatoms on Ag(111). Experiments show that $J(d)$ can be quantitatively described by $J(d) = C_\Delta/d^2$, with $C_\Delta \approx 290$ meV nm^2 [67]. We conducted a search across all 2D space groups and found over 2000 flat-band lattices, including more than 400 strict-flat-band lattices. This confirms the validity of our approach and the abundance of the flat-band lattices. The list of $(1/d^2)$-dependence design results is summarized in SM Table SI. All the structure and band details of the flat-band lattices are listed in the SM.

As demonstrated above, abundant flat-band lattices can be generated using our method. Extending this approach to higher dimensions, multiple types of atoms, multiple electron orbitals, or even incorporating other techniques such as first-principles methods is feasible. Here, we verify the expansibility of the SA-FB generator through first-principles calculations of lattices composed of one or more types of real atoms.

For simplicity, we choose two different kinds of atoms, Na and Rb atoms, to generate flat-band lattices. Both of these atoms have their outermost electron shells filled by s orbitals. Rb is chosen because it is commonly used in cold atom experiments. The first-principles calculations are performed using the Vienna *Ab Initio* Simulation Package (VASP) [60]. The NN distances between atoms are set far enough to ensure that the energy bands near the Fermi energy primarily originate mainly from the overlap of the outermost s orbitals ($3s$ for Na, $5s$ for Rb). Since using VASP calculations at every step will be time-consuming, we calculate $J(d)$ with VASP and use it as an input for the SA-FB generator. For the hopping between the same type of atoms, $J(d)$ is obtained by comparing the tight-binding calculation with the bands calculated using VASP for simple square lattices with different lattice constants. The hopping between Na and Rb is determined using various sized honeycomb like structures with alternating Na and Rb atoms (SM Note 8). Figure 3 shows two examples validated by VASP. The Na flat-band lattice generated by the tight-binding model contains three flat bands at ~0.29, 0.19, and −0.05 eV, respectively. One of them is retained in the VASP calculation at ~ -0.08 eV [see Figs. 3(a) and 3(c)]. The Na and Rb flat-band lattice contains three flat bands at similar energies in both the tight-binding model and VASP [see Figs. 3(d) and 3(f)]. The detailed similarities and differences between the bands calculated with the tight-binding model and VASP can be better visualized in the 2D display shown in SM Note 8. Despite minor differences, the close similarity demonstrates the feasibility of extending the SA-FB generator to first-principles calculations in real atom systems. The slight differences may originate from the influence of the inner shell electrons, which are absent in the tight-binding method but present in VASP. As demonstrated for Na and Rb flat-band lattices, our SA-FB generator can work for different materials as the distance-dependent hopping is an adjustable input parameter, adaptable from the experiments or first-principles calculations.

Before the summary, we briefly compare our SA-FB generator with previous methods. First, similar to previous methods, our new method can generate all the well-known flat-band lattices such as the Lieb, kagome, breathing Kagome [68,69], honeycomb-kagome [70–72], breathing honeycomb-kagome [73], kagome-honeycomb [67,74], and extended Lieb lattices [75] (SM Fig. S13). Second, previous methods, except those searching through existing materials, only generated a few additional flat-band lattices beyond these well-known ones. We also compared our results with the k-uniform tiling flat-band lattices obtained by the brute-force method for the number of sites smaller than 13 and found that all can be found with our SA-FB generator. Our SA flat-band lattice generator can essentially reproduce these lattices, except for those with special requirements (SM Fig. S14
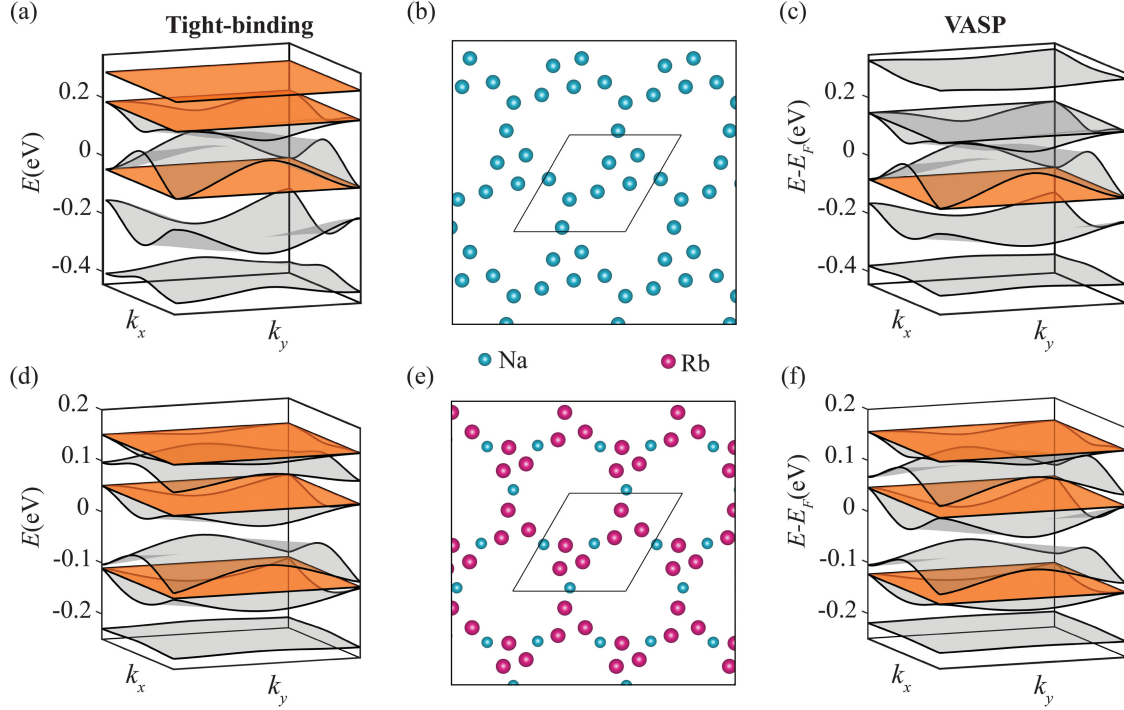
FIG. 3. Flat-band lattices composed of Na and Rb atoms (Details of the atom arrangement are presented in SM Table SII). (a) Energy band containing three flat bands at ~ 0.29, 0.19, and -0.05 eV, respectively, calculated using the tight-binding model for a Na flat-band lattice designed by our SA-FB generator with the structure shown in (b). (c) Energy bands calculated using VASP for the same lattice shown in (b), where one of the flat bands at ~ -0.08 eV from the tight-binding model is maintained. (d) Energy bands with three flat bands at ~ 0.15, 0.05, and -0.11 eV calculated using the tight-binding model for a designed Na and Rb flat-band lattice, with the structure shown in (e). (f) Energy bands calculated using VASP for the lattice shown in (e), where all three flat bands are maintained at similar energies. All flat bands are highlighted in orange.

and Table SIII). Third, our SA-FB generator can produce several hundred strict-flat-band lattices, a number far exceeding those predicted by any previous method.

In summary, we developed a general methodology for constructing 2D flat-band lattices. By formulating the problem of designing flat-band lattices as a mathematical optimization task and applying the distance-dependent hopping and space group symmetry constraints to reduce the problem size, we gradually flattened the dispersive bands into flat bands, alleviating the complexity of the task. The SA-FB generator has rapidly identified more than 1000 2D flat-band lattices. Our results suggested a potentially higher abundance of flat-band lattices than previously anticipated. Furthermore, we found that systems with higher-order NN hopping can produce more flat-band lattices, contrary to the general impression that higher-order NN hopping would destroy flat bands.

[1] D. Leykam, A. Andreanov, and S. Flach, Artificial flat band systems: From lattice models to experiments, Adv. Phys. **3**, 1473052 (2018).

[2] J.-W. Rhim and B.-J. Yang, Singular flat bands, Adv. Phys. **6**, 1901606 (2021).

[3] L. Balents, C. R. Dean, D. K. Efetov, and A. F. Young, Superconductivity and strong correlations in moiré flat bands, Nat. Phys. **16**, 725 (2020).

[4] O. Derzhko, J. Richter, and M. Maksymenko, Strongly correlated flat-band systems: The route from Heisenberg spins to Hubbard electrons, Int. J. Mod. Phys. B **29**, 1530007 (2015).

[5] X. Huang, X. Han, Y. Dai, X. Xu, J. Yan, M. Huang, P. Ding, D. Zhang, H. Chen, V. Laxmi, X. Wu, L. Liu, Y. Wang, Y. Xu, and Y. Huang, Recent progress on fabrication and flat-band physics in 2D transition metal dichalcogenides moiré superlattices, J. Semicond. **44**, 011901 (2023).

[6] D. M. Kennes, L. Xian, M. Claassen, and A. Rubio, One-dimensional flat bands in twisted bilayer germanium selenide, Nat. Commun. **11**, 1124 (2020).

[7] N. Verma, T. Hazra, and M. Randeria, Optical spectral weight, phase stiffness, and Tc bounds for trivial and topological flat band superconductors, Proc. Natl. Acad. Sci. U.S.A. **118**, e2106744118 (2021).

[8] E. H. Lieb, Two theorems on the Hubbard model, Phys. Rev. Lett. **62**, 1201 (1989).

[9] A. Mielke, Ferromagnetism in the Hubbard model on line graphs and further considerations, J. Phys. A **24**, 3311 (1991).

[10] D. Leykam, J. D. Bodyfelt, A. S. Desyatnikov, and S. Flach, Localization of weakly disordered flat band states, Eur. Phys. J. B **90**, 1 (2017).

[11] A. Ahmed, A. Ramachandran, I. M. Khaymovich, and A. Sharma, Flat band based multifractality in the all-band-flat diamond chain, Phys. Rev. B **106**, 205119 (2022).

[12] R. Chen, D.-H. Xu, and B. Zhou, Disorder-induced topological phase transitions on Lieb lattices, Phys. Rev. B **96**, 205304 (2017).

[13] Y. Wang, L. Zhang, Y. Wan, Y. He, and Y. Wang, Two-dimensional vertex-decorated Lieb lattice with exact mobility edges and robust flat bands, Phys. Rev. B **107**, L140201 (2023).

[14] C. Danieli, A. Maluckov, and S. Flach, Compact discrete breathers on flat-band networks, Low Temp. Phys. **44**, 678 (2018).

[15] R. Mondaini, G. G. Batrouni, and B. Grémaud, Pairing and superconductivity in the flat band: Creutz lattice, Phys. Rev. B **98**, 155142 (2018).

[16] D. Călugăru, A. Chew, L. Elcoro, Y. Xu, N. Regnault, Z.-D. Song, and B. A. Bernevig, General construction and topological classification of crystalline flat bands, Nat. Phys. **18**, 185 (2022).

[17] N. Regnault, Y. Xu, M.-R. Li, D.-S. Ma, M. Jovanovic, A. Yazdani, S. S. P. Parkin, C. Felser, L. M. Schoop, N. P. Ong, R. J. Cava, L. Elcoro, Z.-D. Song, and B. A. Bernevig, Catalogue of flat-band stoichiometric materials, Nature (London) **603**, 824 (2022).

[18] H. Liu, S. Meng, and F. Liu, Screening two-dimensional materials with topological flat bands, Phys. Rev. Mater. **5**, 084203 (2021).

[19] F. Crasto de Lima and A. Fazzio, Emergent quasiparticles in Euclidean tilings, Nanoscale **13**, 5270 (2021).

[20] F. Crasto de Lima, G. J. Ferreira, and R. H. Miwa, Topological flat band, Dirac fermions and quantum spin Hall phase in 2D Archimedean lattices, Phys. Chem. Chem. Phys. **21**, 22344 (2019).

[21] R. G. Dias and J. D. Gouveia, Origami rules for the construction of localized eigenstates of the Hubbard model in decorated lattices, Sci. Rep. **5**, 16852 (2015).

[22] S. Flach, D. Leykam, J. D. Bodyfelt, P. Matthies, and A. S. Desyatnikov, Detangling flat bands into Fano lattices, Europhys. Lett. **105**, 30001 (2014).

[23] W. Maimaiti, A. Andreanov, and S. Flach, Flat-band generator in two dimensions, Phys. Rev. B **103**, 165116 (2021).

[24] T. Ogata, M. Kawamura, and T. Ozaki, Methods for constructing parameter-dependent flat-band lattices, Phys. Rev. B **103**, 205119 (2021).

[25] C. S. Chiu, D.-S. Ma, Z.-D. Song, B. A. Bernevig, and A. A. Houck, Fragile topology in line-graph lattices with two, three, or four gapped flat bands, Phys. Rev. Res. **2**, 043414 (2020).

[26] D.-S. Ma, Y. Xu, C. S. Chiu, N. Regnault, A. A. Houck, Z. Song, and B. A. Bernevig, Spin-orbit-induced topological flat bands in line and split graphs of bipartite lattices, Phys. Rev. Lett. **125**, 266403 (2020).

[27] S. Miyahara, K. Kubo, H. Ono, Y. Shimomura, and N. Furukawa, Flat-bands on partial line graphs–Systematic method for generating flat-band lattice structures–, J. Phys. Soc. Jpn. **74**, 1918 (2005).

[28] L. Morales-Inostroza and R. A. Vicencio, Simple method to construct flat-band lattices, Phys. Rev. A **94**, 043831 (2016).

[29] A. Ramachandran, A. Andreanov, and S. Flach, Chiral flat bands: Existence, engineering, and stability, Phys. Rev. B **96**, 161104(R) (2017).

[30] M. Röntgen, C. V. Morfonios, and P. Schmelcher, Compact localized states and flat bands from local symmetry partitioning, Phys. Rev. B **97**, 035161 (2018).

[31] C. V. Morfonios, M. Röntgen, M. Pyzh, and P. Schmelcher, Flat bands by latent symmetry, Phys. Rev. B **104**, 035105 (2021).

[32] C.-C. Lee, A. Fleurence, Y. Yamada-Takamura, and T. Ozaki, Hidden mechanism for embedding the flat bands of Lieb, kagome, and checkerboard lattices in other structures, Phys. Rev. B **100**, 045150 (2019).

[33] H.-Z. Zhang, W.-J. Wu, L. Zhou, Z. Wu, and J. Zhu, Steering on degrees of freedom of 2D van der Waals heterostructures, Small Sci. **2**, 2100033 (2022).

[34] M. Kapfer *et al.*, Programming twist angle and strain profiles in 2D materials, Science **381**, 677 (2023).

[35] A. Rozen, J. M. Park, U. Zondiner, Y. Cao, D. Rodan-Legrain, T. Taniguchi, K. Watanabe, Y. Oreg, A. Stern, E. Berg, P. Jarillo-Herrero, and S. Ilani, Entropic evidence for a Pomeranchuk effect in magic-angle graphene, Nature (London) **592**, 214 (2021).

[36] J. M. Park, Y. Cao, L.-Q. Xia, S. Sun, K. Watanabe, T. Taniguchi, and P. Jarillo-Herrero, Robust superconductivity in magic-angle multilayer graphene family, Nat. Mater. **21**, 877 (2022).

[37] Q. Du, Z. Wang, S. Zhou, J. Zhao, and V. Kumar, Searching for cluster Lego blocks for three-dimensional and two-dimensional assemblies, Phys. Rev. Mater. **5**, 066001 (2021).

[38] B. Cho and Y. Kim, Preparation and properties of 2D materials, Nanomaterials **10**, 764 (2020).

[39] L. Sun, W. Wang, and H. Yang, Recent progress in synaptic devices based on 2D materials, Adv. Intell. Syst. **2**, 1900167 (2020).

[40] F. He, Y. Zhou, Z. Ye, S.-H. Cho, J. Jeong, X. Meng, and Y. Wang, Moiré patterns in 2D materials: A review, ACS Nano **15**, 5944 (2021).

[41] P. Ares and K. S. Novoselov, Recent advances in graphene and other 2D materials, Nano Mater. Sci. **4**, 3 (2022).

[42] X. Li, Q. Li, T. Ji, R. Yan, W. Fan, B. Miao, L. Sun, G. Chen, W. Zhang, and H. Ding, Lieb lattices formed by real atoms on Ag(111) and their lattice constant-dependent electronic properties, Chin. Phys. Lett. **39**, 057301 (2022).

[43] R. Drost, T. Ojanen, A. Harju, and P. Liljeroth, Topological states in engineered atomic lattices, Nat. Phys. **13**, 668 (2017).

[44] L. Yan and P. Liljeroth, Engineered electronic states in atomically precise artificial lattices and graphene nanoribbons, Adv. Phys. **4**, 1651672 (2019).

[45] M. R. Slot, S. N. Kempkes, E. J. Knol, W. M. J. van Weerdenburg, J. J. van den Broeke, D. Wegner, D. Vanmaekelbergh, A. A. Khajetoorians, C. Morais Smith, and I. Swart, *p*-band engineering in artificial electronic lattices, Phys. Rev. X **9**, 011009 (2019).

[46] L. Kormoš, P. Procházka, A. O. Makoveev, and J. Čechal, Complex k-uniform tilings by a simple bitopic precursor self-assembled on Ag(001) surface, Nat. Commun. **11**, 1856 (2020).

[47] Y. Shuku, R. Suizu, S. Nakano, M. Tsuchiizu, and K. Awaga, Engineering Dirac cones and topological flat bands with organic molecules, Phys. Rev. B **107**, 155123 (2023).

[48] L. Feng, T. Wang, Z. Tao, J. Huang, G. Li, Q. Xu, S. L. Tait, and J. Zhu, Supramolecular tessellations at surfaces by vertex design, ACS Nano **13**, 10603 (2019).

[49] F. Cheng, X.-J. Wu, Z. Hu, X. Lu, Z. Ding, Y. Shao, H. Xu, W. Ji, J. Wu, and K. P. Loh, Two-dimensional tessellation by molecular tiles constructed from halogen–halogen and halogen–metal networks, Nat. Commun. **9**, 4871 (2018).

[50] H. Wang, P. Fan, J. Chen, L. Jiang, H.-J. Gao, J. L. Lado, and K. Yang, Construction of topological quantum magnets from atomic spins on surfaces, Nat. Nanotechnol. **19**, 1782 (2024).

[51] L. Song, Y. Xie, S. Xia, L. Tang, D. Song, J.-W. Rhim, and Z. Chen, Topological flatband loop states in fractal-like photonic lattices, Laser Photonics Rev. **17**, 2200315 (2023).

[52] J.-P. Lang, H. Hanafi, J. Imbrock, and C. Denz, Tilted Dirac cones and asymmetric conical diffraction in photonic Lieb-kagome lattices, Phys. Rev. A **107**, 023509 (2023).

[53] C. Chen, L. Qi, K.-X. Hu, J. Cao, W.-X. Cui, S. Zhang, and H.-F. Wang, Magnetic-flux-induced tunable completely flat band and topological nearly flat band in square kagome lattice, Ann. Phys. (Amsterdam) **535**, 2200645 (2023).

[54] J. Wang, Y. Peng, H. Xu, J. Feng, Y. Huang, J. Wu, T. C. H. Liew, and Q. Xiong, Controllable vortex lasing arrays in a geometrically frustrated exciton–polariton lattice at room temperature, Natl. Sci. Rev. **10**, nwac096 (2023).

[55] K. Deligiannis, Q. Fontaine, D. Squizzato, M. Richard, S. Ravets, J. Bloch, A. Minguzzi, and L. Canet, Kardar-Parisi-Zhang universality in discrete two-dimensional driven-dissipative exciton polariton condensates, Phys. Rev. Res. **4**, 043207 (2022).

[56] C. Wang, Y. Zhang, and V. V. Konotop, Wannier solitons in spin-orbit-coupled Bose-Einstein condensates in optical lattices with a flat band, Phys. Rev. A **108**, 013307 (2023).

[57] D. A. Zezyulin and V. V. Konotop, Localization of ultracold atoms in Zeeman lattices with incommensurate spin-orbit coupling, Phys. Rev. A **105**, 063323 (2022).

[58] H. Li, Z. Dong, S. Longhi, Q. Liang, D. Xie, and B. Yan, Aharonov-Bohm caging and inverse Anderson transition in ultracold atoms, Phys. Rev. Lett. **129**, 220403 (2022).

[59] See Supplemental Material at http://link.aps.org/supplemental/10.1103/PhysRevLett.134.076402 for details of the SA-FB generator algorithm, summary of all generated flat-band lattices, and details of first-principles calculations, which includes Refs. [16,21–32,60–62].

[60] G. Kresse and J. Furthmüller, Efficiency of ab-initio total energy calculations for metals and semiconductors using a plane-wave basis set, Comput. Mater. Sci. **6**, 15 (1996).

[61] P. E. Blöchl, Projector augmented-wave method, Phys. Rev. B **50**, 17953 (1994).

[62] J. P. Perdew, K. Burke, and M. Ernzerhof, Generalized gradient approximation made simple, Phys. Rev. Lett. **77**, 3865 (1996).

[63] C. Kittel, *Introduction to Solid State Physics*, 8th ed. (Wiley, New York, 2004).

[64] D. Bertsimas and J. Tsitsiklis, Simulated annealing, Stat. Sci. **8**, 10 (1993).

[65] R. A. Rutenbar, Simulated annealing algorithms: An overview, IEEE Circuits Dev. Mag. **5**, 19 (1989).

[66] S. Kirkpatrick, C. D. Gelatt, and M. P. Vecchi, Optimization by simulated annealing, Science **220**, 671 (1983).

[67] R. G. Yan, T. Z. Ji, W. L. Fan, Z. X. Zhang, H. T. Li, L. Sun, B. F. Miao, G. Chen, and H. F. Ding, Experimental demonstration of the band compression effect in engineered kagome-honeycomb lattices, Phys. Rev. B **108**, 075153 (2023).

[68] A. Bolens and N. Nagaosa, Topological states on the breathing kagome lattice, Phys. Rev. B **99**, 165141 (2019).

[69] M. Ezawa, Higher-order topological insulators and semimetals on the breathing kagome and pyrochlore lattices, Phys. Rev. Lett. **120**, 026801 (2018).

[70] W. Maimaiti, B. Dietz, and A. Andreanov, Microwave photonic crystals as an experimental realization of a combined honeycomb-kagome lattice, Phys. Rev. B **102**, 214301 (2020).

[71] A. Hashmi, K. Nakanishi, M. U. Farooq, and T. Ono, Ising ferromagnetism and robust half-metallicity in two-dimensional honeycomb-kagome Cr2O3 layer, npj 2D Mater. Appl. **4**, 39 (2020).

[72] X.-B. Wang, B. Xia, C.-K. Lyu, D. Kim, E. Li, S.-Q. Fu, J.-Y. Chen, P.-N. Liu, F. Liu, and N. Lin, A p-orbital honeycomb-Kagome lattice realized in a two-dimensional metal-organic framework, Commun. Chem. **6**, 73 (2023).

[73] L. Liu, B. Zhao, J. Zhang, H. Bao, H. Huan, Y. Xue, Y. Li, and Z. Yang, Prediction of coexistence of anomalous valley Hall and quantum anomalous Hall effects in breathing kagome-honeycomb lattices, Phys. Rev. B **104**, 245414 (2021).

[74] M. Telychko, G. Li, P. Mutombo, D. Soler-Polo, X. Peng, J. Su, S. Song, M. J. Koh, M. Edmonds, P. Jelínek, J. Wu, and J. Lu, Ultrahigh-yield on-surface synthesis and assembly of circumcoronene into a chiral electronic Kagome-honeycomb lattice, Sci. Adv. **7**, eabf0269 (2021).

[75] A. Bhattacharya and B. Pal, Flat bands and nontrivial topological properties in an extended Lieb lattice, Phys. Rev. B **100**, 235145 (2019).